Characterization of Continuously Distributed Cortical Water Diffusion Rates With a Stretched-Exponential Model

Kevin M. Bennett,[1] Kathleen M. Schmainda,[1,2] Raoqiong Bennett (Tong),[3] Daniel B. Rowe,[1] Hanbing Lu,[1] and James S. Hyde[1*]

Experience with diffusion-weighted imaging (DWI) shows that signal attenuation is consistent with a multicompartmental theory of water diffusion in the brain. The source of this so-called nonexponential behavior is a topic of debate, because the cerebral cortex contains considerable microscopic heterogeneity and is therefore difficult to model. To account for this heterogeneity and understand its implications for current models of diffusion, a stretched-exponential function was developed to describe diffusion-related signal decay as a continuous distribution of sources decaying at different rates, with no assumptions made about the number of participating sources. DWI experiments were performed using a spin-echo diffusion-weighted pulse sequence with *b*-values of 500–6500 s/mm^2 in six rats. Signal attenuation curves were fit to a stretched-exponential function, and 20% of the voxels were better fit to the stretched-exponential model than to a biexponential model, even though the latter model had one more adjustable parameter. Based on the calculated intravoxel heterogeneity measure, the cerebral cortex contains considerable heterogeneity in diffusion. The use of a distributed diffusion coefficient (DDC) is suggested to measure mean intravoxel diffusion rates in the presence of such heterogeneity. Magn Reson Med 50: 727–734, 2003. © 2003 Wiley-Liss, Inc.

Key words: diffusion; stretched-exponential; brain; model; multi-exponential

Two types of heterogeneity can be defined in MRI diffusion experiments: intravoxel and intervoxel. The goal of this work was to understand how intravoxel heterogeneity affects measurements of diffusion in the cerebral cortex using diffusion-weighted imaging (DWI). A stretched-exponential model was used to study the heterogeneity in DWI data.

The motivation for understanding the biophysical basis of DWI lies partially in the potential of the technique for noninvasively detecting microscopic changes in tissue due to cerebral infarction and stroke (1). In addition, DWI studies of the changes in restrictions to intra- and extracellular water diffusion that occur with neoplastic invasion may lead to improved understanding and treatment of tumors (2,3). Finally, it has been shown that a reduction in the apparent diffusion coefficient (ADC) may occur during functional stimulation, which suggests the use of DWI as a functional contrast technique to study brain activation (4).

Mathematical models of DWI have been tested in humans, animals, and cell cultures, but the controversy surrounding the identification of specific proton pools contributing to nonexponential behavior of the neural DWI signal remains (5–11). In vitro models, such as erythrocyte ghosts (10), have done much to establish the sensitivity of multiexponential models to cellular density, volume fractions, and exchange rates. However, the direct correspondence of these models to the results of brain imaging must still be established.

The biexponential model of water diffusion assumes that there are two distinct proton pools inside each voxel, and that these proton pools have different diffusion rates that result in signal relaxation with b that is biexponential, where $b = \gamma^2 G^2 \delta^2 (\Delta - \delta/3)$. The variable G is the magnitude of the applied diffusion gradient, δ is the duration of each lobe of the diffusion gradients, Δ is the time between the onsets of the two gradient pulses, and γ is the gyromagnetic ratio. When δ is not negligibly smaller than Δ, the diffusion time for the experiment can be written as $t_d = \Delta - \delta/3$ (12). The form of the biexponential model is

$$\frac{S(b)}{S_0} = V_1 e^{-b D_1} + V_2 e^{-b D_2}, \qquad [1]$$

where $S(b)/S_0$ is the component of signal attenuation caused by diffusion through the applied magnetic field gradients. The parameters V_1 and V_2 are the volume fractions in fast- and slow-diffusing "compartments", such that $V_1 + V_2 = 1$. Parameters D_1 and D_2 are the corresponding ADCs. There are three independent parameters in the model of Eq. [1]: V_1/V_2, D_1, and D_2.

It has been suggested that V_1 and V_2 are the volume fractions of protons in the extra- and intracellular spaces, respectively, in the neural cortex (6). However, the biexponential model is confounded by a reported mismatch between expected volume fractions and fitted results from the DWI data, namely a reversal of the expected volume fractions of the slow- and fast-diffusing components (6,7). Possible explanations for this mismatch are exchange between proton pools (13), and the existence of multiple pools within the region of interest (ROI). Experiments have borne out the effects of these phenomena on biexponential fits to data from isolated (nonliving or cultured) systems (10,11). It has been found, however, that in vitro diffusion

[1]Department of Biophysics, Medical College of Wisconsin, Milwaukee, Wisconsin.

[2]Department of Radiology, Medical College of Wisconsin, Milwaukee, Wisconsin.

[3]GE Medical Systems, Milwaukee, Wisconsin.

Grant sponsor: National Institutes of Health; Grant numbers: CA-82500-01; MH51358; EB00215.

*Correspondence to: James S. Hyde, Department of Biophysics, Medical College of Wisconsin, 8701 Watertown Plank Rd., Milwaukee, WI 53226. E-mail: jshyde@mcw.edu

Received 6 January 2003; revised 28 May 2003; accepted 28 May 2003.

DOI 10.1002/mrm.10581

Published online in Wiley InterScience (www.interscience.wiley.com).

images of single oocytes yield biexponential curves from intracellular signal alone, challenging the idea that V_1 and V_2 correspond to intra- and extracellular proton pools (9). One possible cause of this dilemma is the highly heterogeneous nature of cortical tissue. The neocortex of mammals is composed of six identifiable layers, each of which contains a varying proportion of axonal and dendritic projections from subcortical and neighboring cortical structures (14,15), as well as associated glial cells. Mono- or bicompartmental signal models may have a physical basis in separate parenchymal proton pools, but one must also consider the possibility that a continuous distribution of diffusion coefficients arises from a multiplicity of pools (16).

In this study a model was developed, based on the theory of the stretched-exponential function, in which no assumption was made about the number of intravoxel proton pools contributing to signal decay. As a rule, deconvolution of a decaying exponential-like signal into monoexponential components is possible only when extra information exists about the number of exponentials. In the absence of this information, the stretched exponential provides a means of characterizing the decay, and the resultant fitted parameters can be used to quantify the intravoxel distribution of apparent diffusion rates.

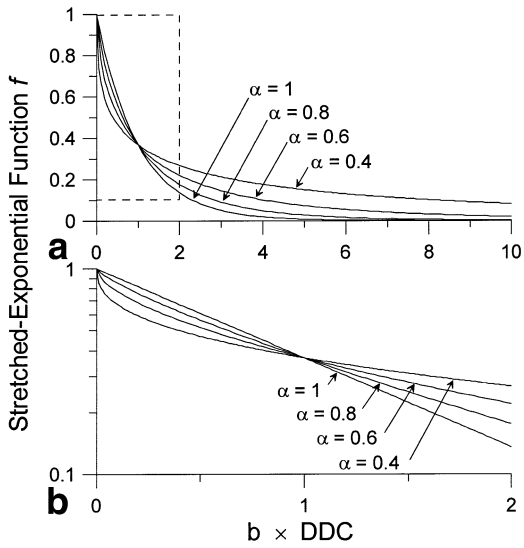

FIG. 1. **a:** Stretched-exponential function $f = S(b)/S_0$ with varying values of α (from upper to lower values of 0.4, 0.6, 0.8, and 1.0). **b:** Enlargement of the area in dashed lines of **a**, in a semilog (y) scale.

THEORY

If the ROI is composed of a collection of protons with a distribution of (apparent) diffusion coefficients, the equations relating diffusion to MR signal attenuation take on a general form. A probability density $\rho(D)$ is assigned to the populations of protons with a particular D in a voxel. Signal attenuation can then be thought to arise from a collection of uncoupled exponential decay processes, such that:

$$\frac{S(b)}{S_0} = \int_0^\infty \rho(D) e^{-bD}\, dD. \qquad [2]$$

To describe the behavior of the same signal attenuation analytically as a function of b-value, we propose the use of the stretched-exponential model:

$$\frac{S(b)}{S_0} = \exp\{-(b \times \mathrm{DDC})^\alpha\}. \qquad [3]$$

Here α is the stretching parameter, which characterizes the deviation of the signal attenuation from monoexponential behavior, and is limited to values between zero and one. A value of α that is near one indicates high homogeneity in apparent diffusion, namely a highly monoexponential attenuation curve. Lower values of α result from nonexponential behavior caused by the addition of multiple separable proton pools within the voxel. This function, known as the Kohlrausch-Williams-Watts model, has been applied extensively in other fields of physics to problems similar to the one addressed here (17–22), and was used to describe nonexponential diffusion in neural tissue specimens (23). There are two free parameters in the model of Eq. [3]: the distributed diffusion coefficient (DDC) and α. The DDC parameter refers to the quantity derived from fitting the stretched-exponential function to the data. In Eqs. [2] and [3], DDC and D are dependent, as are the biexponential estimates of diffusion rates in Eq. [1], on the time allowed for diffusion. They do not directly reflect the fluid viscosity unless diffusion is unrestricted.

As shown in Fig. 1a, a decrease in α results in a decrease in signal attenuation as a function of b-value if $b \times \mathrm{DDC} > 1$. If $b \times \mathrm{DDC} < 1$, the opposite effect occurs, such that low α values result in a relatively fast signal decay. Thus, the form of Eq. [3] accommodates a range of decay rates as described by Eq. [2]. The parameter $b \times \mathrm{DDC}$ determines the point at which these curves cross each other, effectively delineating "high" and "low" ranges of decay rates. If $b \times \mathrm{DDC}$ is high, the signal attenuation is dominated by the slow-decaying terms, since faster-decaying contributions have already disappeared. The "stretching" behavior to which the model refers is seen at high values of $b \times \mathrm{DDC}$, where a lower α prevents the function from decaying quickly. Low values of α signify that a large number of disparate apparent diffusion rates are present in the sample. In a semilogarithmic plot of the signal attenuation curve (Fig.1b), more than one decay term (slope of $\log(S(b)/S_0)$), can clearly be seen if $\alpha < 1$, although the behavior does not arise from a specific number of decay components.

The signal attenuation of Eq. [2] can be defined in a slightly different way. Let $\beta = 1/D$, (which has the same units as b – s/mm^2), where β can be thought of as a decay constant resulting from the apparent diffusion rate D. The parameter D is a continuously varying ADC. Following the method described in Ref. 22, the modeled values of DDC, α, and β are related by equating the right-hand sides of Eq. [2] and Eq. [3]:

$$e^{-(b\times \mathrm{DDC})^{\alpha}} = \int_0^{\infty} \rho(\beta) e^{-(b/\beta)}\, d\beta. \quad [4]$$

Let $E(\beta^n)$ be the nth moment of the distribution of $1/D$, which can then be calculated by integrating $\beta^n\rho(\beta)$ over its range. Thus

$$E(\beta^n) = \frac{1}{\mathrm{DDC}^n\alpha}\frac{\Gamma\left(\frac{n}{\alpha}\right)}{\Gamma(n)}, \quad [5]$$

which, for the first moment of β, is

$$E(\beta) = \frac{1}{\mathrm{DDC}\,\alpha}\Gamma\left(\frac{1}{\alpha}\right). \quad [6]$$

Thus, $E(\beta)$ approaches β as α approaches one. The moments of β can be analyzed to generate information about $\rho(\beta)$. Maps of increasing moments of β progressively increase the weighting of protons with low ADCs.

Figure 2 shows the effects of α and DDC on the first and third moments of β. Higher moments are weighted by lower values of α resulting from heterogeneous decay. Decreasing DDC also results in lower $E(\beta^n)$. Maps of the first three moments of β in each voxel can be created.

There are, therefore, five useful parameters that characterize intravoxel diffusion with this model: α, DDC, and the first three moments of the distribution of β. All of these parameters are obtained in a fit of the stretched-exponential function to the data.

The goal of this work was to understand how intravoxel heterogeneity affects physical interpretation of the DWI signal decay. Because it is sensitive to this heterogeneity, a stretched-exponential model was developed and fitted to the signal attenuation curves of rat brain images. The possibility of obtaining image contrast with the stretched-exponential model of diffusion using maps of α, DDC, and the first three moments of the intravoxel distribution of β was also studied.

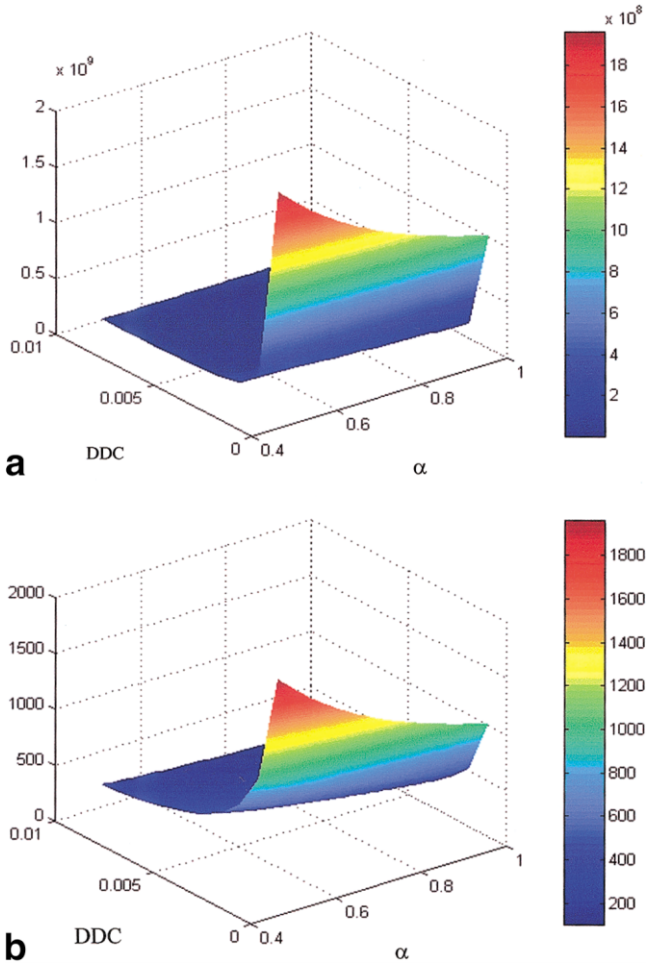

FIG. 2. Surface plots of (**a**) $E(\beta^3)$ and (**b**) $E(\beta)$ as a function of α and DDC. Vertical height is the moment amplitude and is labeled in the corresponding color bars for each figure.

MATERIALS AND METHODS

Eight male Sprague-Dawley rats were imaged using a spin-echo DW (spin-warp) pulse sequence. While echo-planar pulse sequences would have allowed more rapid image acquisition, the newness of the analysis method encouraged caution with regard to the effects of T_2^* decay and eddy currents on signal intensity. The rats were anesthetized with urethane (1.2 mg/kg of 20% solution) during the scan, and their core temperatures were maintained at 37°C ± 0.5°C before and during the experiment. The rats were handled in accordance with the NIH *Guide for the Use and Care of Laboratory Animals*. A Bruker Biospec 3T scanner was used to acquire the images, with a local 12-cm gradient coil, (12.8-cm inner diameter, 41.0-cm length, maximum gradient amplitude of 20 G/cm at 100A for each axis, rise times ≤ 100 μs), and a single-turn square surface RF coil of 2 cm^2 area. A 64 × 64 matrix, a FOV of 3.5 cm, five axial slices of 1.0-mm thickness, and a TE of 43 ms were used. The pulse sequence incorporated a 90° and a 180° RF pulse, with a magnetic field gradient applied before and after the RF pulses for diffusion weighting. A single *k*-space line was acquired with each excitation. The *b*-value was varied from 0 to 6500 s/mm^2 in increments of 500 s/mm^2 by varying the amplitude of the two gradient pulses after the 90° and after 180° RF pulses. The diffusion gradients were applied in the frequency-encoding direction. The diffusion time was 27 ms, and the *b*-values were varied randomly according to a uniform distribution to avoid systematic errors. The signal attenuation ratio was calculated in each voxel by dividing the DWI signal by the T_2-weighted ($b = 0$) signal. The cortical ribbon was localized visually from a T_2-weighted (TR = 1400 ms, TE = 19 ms) anatomical image acquired prior to DWI, and an ROI was created manually to contain voxels inside cerebral cortex in each rat. Two magnitude images were acquired with each *b*-value and averaged to produce the final image. If the magnitude-to-noise ratio was less than 3, the images were excluded from the final analysis.

Bi- and stretched-exponential models were fitted to the data from each voxel in the ROI using a nonlinear least-squares routine in Matlab (Mathworks, Inc.). A Gauss-Newton method was applied, with bounds on the

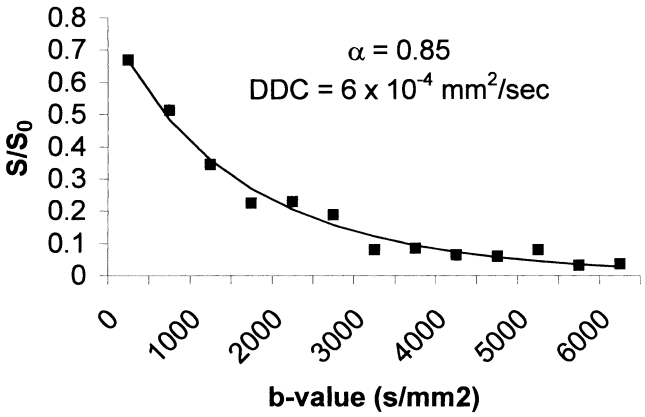

FIG. 3. Typical signal attenuation data (taken from a voxel in images of cerebral cortex of a male Sprague-Dawley rat), as a function of *b*-value. The stretched-exponential fit to the data is shown as a solid line in the figure.

stretched-exponential parameters as follows: $0 < \text{DDC} < 10 \times 10^{-3}$ s/mm^2, and $0 < \alpha < 1$. The biexponential parameters were specified such that $V_1 + V_2 = 1$, $0 < V_1 < 0.4$, $0 < D_1 < 10 \times 10^{-3}$ mm^2/s, and $0 < D_2 < 10 \times 10^{-3}$ mm^2/s. The fitting algorithm converged if the results changed by less than a specified amount with an incremental change in the parameter set, and a maximum of 5000 changes in the parameter set were allowed.

The goodness-of-fit of the bi- and stretched-exponential models to the data were compared. An equal goodness-of-fit would indicate a preference for the stretched-exponential model, assuming there is no prior information about the number of intravoxel proton pools, since the stretched-exponential model contains one less free parameter than does the biexponential model. To compare the models, the sum-of-squared residuals (SSR) was calculated between each fit and the signal attenuation as a function of *b* for each voxel. A monoexponential ADC was also computed in each voxel using the relation ADC = $\ln(S_0/S(b))/b$, with $b = 1000$ s/mm^2.

To assess the behavior of the stretched-exponential model in measuring homogeneity or monoexponential behavior in a system of relatively fast diffusion coefficients, data from a 10% ethanol solution in a 1.5-ml vial were fitted to the stretched-exponential model using the same protocol. It was predicted that α would be higher in the ethanol phantom than in the rat cortex because of the monoexponential signal attenuation from a homogeneous distribution of *D* in the ethanol phantom.

In designing pulse sequences for measuring heterogeneity in diffusion, it is important to know the range of imaging parameters that result in maximum sensitivity to the physical system under investigation. One method for assessing the sensitivity of the model is to calculate the partial derivative of the model with respect to the variable of interest. This technique was used to determine how the sensitivity of the model to α was related to the diffusion coefficients present in the sample, and how this sensitivity was controlled by the magnitude of the applied diffusion gradients. An analytical simulation was written in Matlab to vary α from 0.2 to 1.0 in increments of 0.2, with $b \times$ DDC specified between 0 and 10. The partial derivative of the modeled signal attenuation $f = S(b)/S_o$ was calculated with respect to α.

RESULTS

One of the eight rats imaged experienced bleeding due to surgical complications during the scan, and another rat experienced uncontrollable temperature fluctuations. The data from both of these rats were excluded from the final analysis. The results of the stretched-exponential fit to 99 voxels from the ethanol phantom indicated homogeneous (monoexponential) signal attenuation in every voxel. The mean value of α was 0.97, with a median of 0.98 and a standard deviation (SD) of 0.02. A two-tailed Student's *t*-test comparing the distributions from the rat cortical dataset with that of the ethanol phantom showed statistically significant differences ($P < 0.001$) in all six cases. A typical signal attenuation curve is shown in Fig. 3, along with a stretched-exponential fit to the data.

Figure 4 shows the distribution of the difference of the SSR of the stretched exponential model, SSR_s, to that of the biexponential, SSR_b. Of 3038 voxels, 20% had a lower SSR with the stretched-exponential fit.

The fitted values of α for each rat were calculated from within the ROI. Bins of size 0.05 were selected, and the frequency of voxels in the dataset with α within each bin was computed, as shown in Fig. 5a. The mean value of α was 0.80, with a median of 0.82 and an SD of 0.12. The distribution DDC ($7.5 \times 10^{-4} \pm 3.4 \times 10^{-4}$ mm^2/s) from the same fits is shown in Fig. 5b. The results of stretched-exponential fits for every rat are shown in Table 1, with ADC ($b = 1000$ s/mm^2) values listed for comparison with DDC values.

A map of α fitted to each voxel in cortical ribbon taken from three rats is shown in Fig. 6 along with a typical ROI drawing (left) on a T_2-weighted anatomical image. This

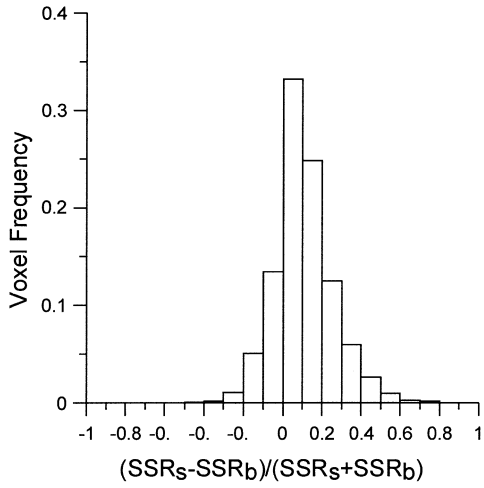

FIG. 4. Histogram analysis of stretched- and bi-exponential fits from voxels taken from images of six healthy rats. The goodness-of-fit is reported between fits of the stretched- and bi-exponential models, with sum-of-squared residuals SSR_s and SSR_b, respectively. Negative values indicate a higher likelihood for the stretched-exponential model (N = 3038).

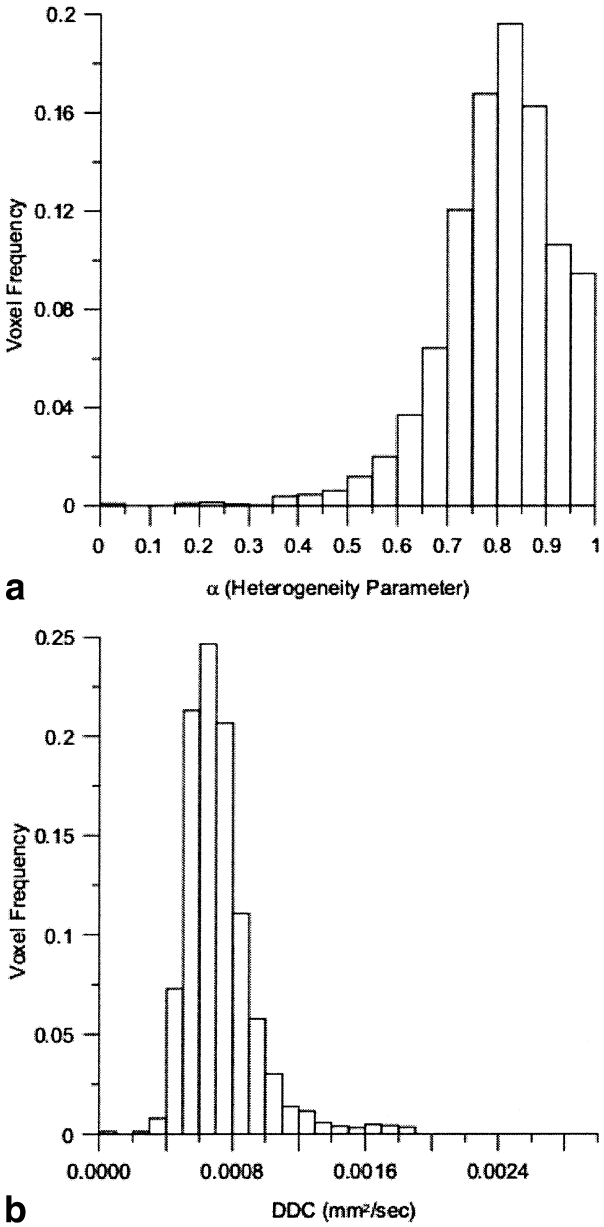

FIG. 5. **a:** Histogram of stretched-exponential heterogeneity measure α in rat cerebral cortex from a nonlinear least-squares fit. Data was obtained from DWI of six male Sprague-Dawley rats. **b:** Histogram of stretched-exponential DDC from the same voxels (N = 3038).

map shows that heterogeneity is generally low in the central and superior (upper) portions of the cortex, and some slices have lowered α in inferior (lower) cortical voxels.

Figure 7 shows a comparison of color images of α, DDC, E(β), E(β^2), and E(β^3) in voxels of whole-brain images. The results show high contrast between white matter structures (e.g., the corpus colossum) and the cortical ribbon, with white-matter tracts having higher DDC, and subcortical structures showing contrast with the moments of β.

DISCUSSION AND CONCLUSIONS

Signal attenuation due to water proton diffusion in DWI has been analyzed using a stretched-exponential function, which assumes that each voxel contains a continuous distribution of diffusion rates. As expected, the heterogeneity parameter α was close to one in stretched-exponential fits to voxels from (freely-diffusing) protons in an ethanol phantom. By comparison, α in rat cerebral cortical voxels was significantly less ($P < 0.001$) in all six rats, supporting the initial hypothesis that the stretched-exponential model could be used to measure heterogeneity in water diffusion.

The stretched-exponential model yielded a measure of the moments of the intravoxel distribution of diffusion coefficients. The moments of β were calculated using the values of DDC and α in each voxel. Maps of DDC, E(β^2), and E(β^3) were created. Further studies must be done to elucidate the relative contributions of higher or lower components of the subvoxel distributions of D between different brain structures; however, these results suggest that a new type of diffusion contrast can be observed with the stretched-exponential technique. Since E(β^3) is sensitive to contributions from low values of D, it can be speculated that signal attenuation resulting in high E(β^3) has origins in the cellular microenvironment.

Figure 8 shows that caution must be used in selecting b-values to match the diffusion coefficients in the sample. The sensitivity of f to α, and therefore to heterogeneity, is dependent upon $b \times$ DDC, and upon α itself. Choosing $b \times$ DDC to be high results in low sensitivity to heterogeneity, because signal attenuation of all but the most heterogeneous diffusion components has occurred. In general, f is more sensitive to α when α is low rather than high, assuming $b \times$ DDC is not close to one.

An interesting observation concerning the stretched-exponential function shown in Fig. 1 is that DDC ≅ ADC (the monoexponential ADC), when $b \times$ DDC ≅ 1. It is understood that both DDC and ADC are affected by the heterogeneity of diffusion rates in the voxel, but that, assuming the point at which $b \times$ DDC = 1 (or S/S_o = 1/e) is known, DDC can be obtained by taking an ADC measurement at that point. The value of DDC is higher when intravoxel diffusion rates are fast and homogeneous. Conversely, E(β^3) is high when the diffusion rates are slow but heterogeneous (low α), as shown in Eq. [6].

A more practical implication is that, in studies where an ROI is defined in order to compare some measure of the diffusion rate to that of surrounding tissue, it is advanta-

Table 1
Results From Stretched-Exponential Fits to Cortex ROIs in Seven Healthy Rats

Rat	DDC (mm^2/s) 10^{-4}	α	ADC (mm^2/s) 10^{-4}
1 (N = 383)	6.8 ± 3.6	0.82 ± 0.10[a]	7.1 ± 2.6
2 (N = 504)	7.6 ± 1.9	0.80 ± 0.15[a]	7.9 ± 1.8
3 (N = 546)	7.8 ± 5.3	0.81 ± 0.15[a]	7.5 ± 4.2
4 (N = 585)	7.5 ± 2.3	0.79 ± 0.09[a]	8.0 ± 2.3
5 (N = 554)	8.0 ± 3.5	0.77 ± 0.10[a]	8.1 ± 2.3
6 (N = 467)	7.2 ± 3.1	0.80 ± 0.11[a]	7.5 ± 2.4

*The monoexponential ADC values (calculated with b = 1000 s/mm^2) are listed for comparison with the DDC values. Results are reported with ± 1 standard deviation.

[a]Results were significantly different ($P < 0.001$) from those of an ethanol phantom.

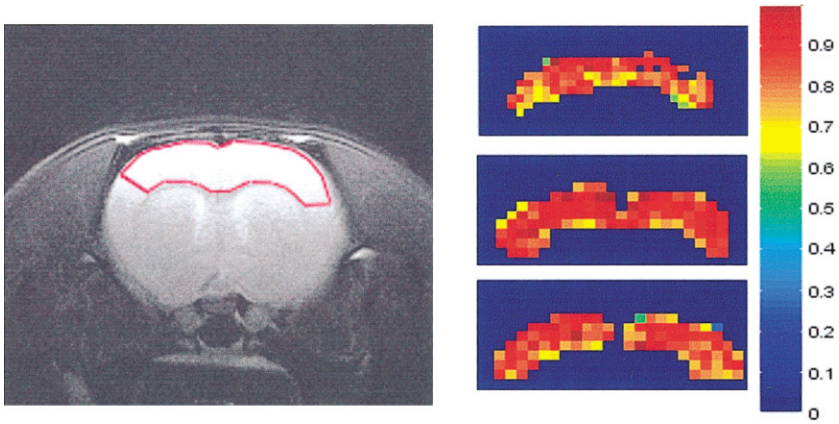

FIG. 6. Color map of the heterogeneity index α in a stretched-exponential fit to signal attenuation from ROI voxels in cerebral cortical ribbon (outlined in the anatomical image at left).

geous to perform ADC measurements with two different *b*-values, each optimized with different $b \times$ DDC (one value for the ROI, and one for surrounding tissue). This may be useful, for instance, in localizing a region of cytotoxic edema following the onset of stroke.

A color map of α in a representative slice taken from rat cerebral cortex showed reduced α in regions corresponding to the superior sagittal sinus. This is thought to occur because of partial volume effects between the relatively fast-diffusing CSF in the sinus and the slow-diffusing gray matter parenchymal protons.

It is possible that the heterogeneity index is sensitive to the direction of the applied diffusion gradients, particularly in highly anisotropic structures in the brain. This is expected because diffusion imaging of the brain has revealed considerable anisotropy (31,32). In the present studies, diffusion gradients were applied in only one direction to avoid averaging the data in more than one direction. In a separate experiment (results not shown), with the diffusion gradient applied in a direction orthogonal to the one employed here (vertical in the images), it was found that the heterogeneity index α was not significantly different than that found using diffusion gradients in the *x*-direction. While further studies are needed to understand the directional dependence of heterogeneity, it appears that the relatively isotropic nature of gray matter lends itself to analysis using gradients in only one direction.

The results of this study enable one to hypothesize that subvoxel heterogeneity measures may provide contrast between motor functional units. Supporting this hypothesis is the fact that somatosensory and motor functional units

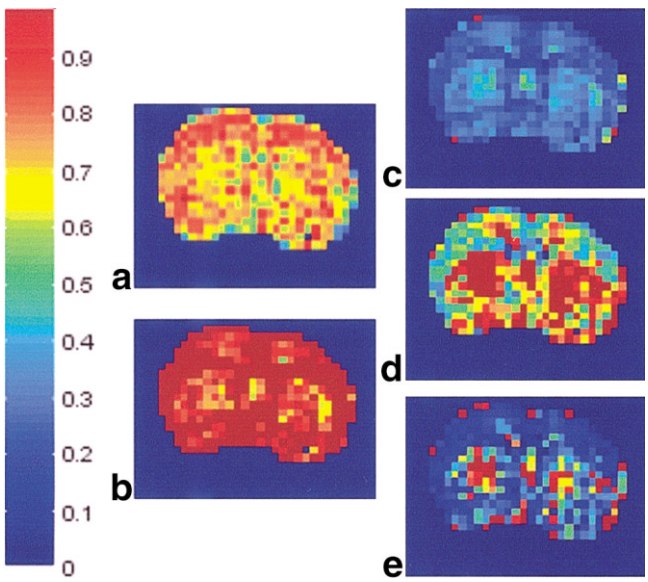

FIG. 7. Color maps of stretched-exponential fits of data from cerebral cortex. **a**: Stretched-exponential fit α; **b**: Stretched-exponential fitDDC; and **c–e**: Moments 1, 2, and 3 of β.

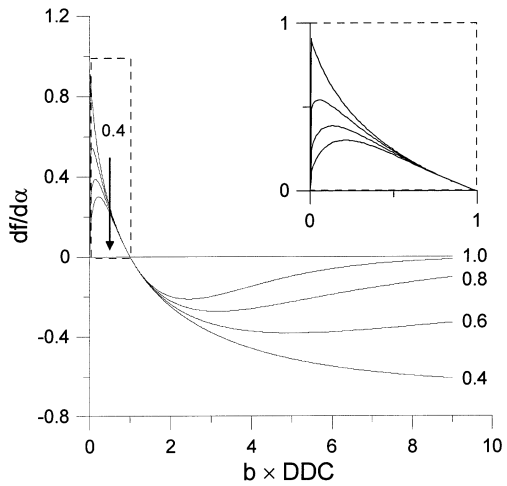

FIG. 8. Sensitivity of the stretched-exponential function *f* (partial derivative) with respect to α as a function of $b \times$ DDC. The arrow indicates an increase in α. The upper-right insert is an enlarged view of the main plot, for $0 \leq b \times \text{DDC} \leq 1$.

(barrels) are approximately 45–60 mm^3 in volume, are separated by distances on the order of the slice thickness that was used, and correspond to the physical location of the slices employed here, as verified by localization of the anatomical slices with a rat brain atlas (24). Barrels extend vertically (S-I) and are separated laterally (in the slice direction) by approximately 1–1.5 mm, in a grid-like pattern. Interconnections between functionally related cortical areas are also heterogeneous from the superior to the inferior direction, and mostly occur in layer IV. There is therefore a potential for the stretched-exponential model of diffusion to be of use in high-resolution imaging. A particular application may involve using the heterogeneity index to track functional disruption due to pathologies.

Q-space imaging is a commonly used DWI technique for obtaining information about subvoxel diffusion. The basis of the technique is that when $\delta < \Delta$, the probability of protons having diffused a distance R is related by the Fourier transform with respect to R to the signal intensity at the echo as a function of q. The variable q is a measure of diffusion weighting under these circumstances, and is defined as $\gamma\delta G/2\pi$ in units of one/distance. By sampling the attenuation curve with different values of q, one can make an estimate of this probability with a fixed diffusion time (Δ). *Q*-space imaging shows promise for the imaging of microscopic structure, particularly when the structure is spatially periodic (28–30). However, in vivo imaging with *q*-space methods, particularly in humans, may be limited by both hardware capabilities (i.e., maximum gradient strength) and safety concerns (e.g., very rapid rise times for the diffusion gradients). The current stretched-exponential method is useful for measuring restricted diffusion in these less than ideal conditions since, in general, δ is not greatly less than Δ.

Two types of intravoxel heterogeneity affect diffusion-related signal attenuation data: heterogeneity in fluid viscosity, and heterogeneity in diffusive restrictions. If diffusion times are short, the former effect dominates the heterogeneity, but longer diffusion times allow protons to experience restrictive barriers. To analyze these two effects, theoretical analysis and experiments were performed in which b was varied by holding the gradient amplitude G constant and varying the diffusion time (25–27). These efforts were partly based on pioneering work by Callaghan (28) in *q*-space imaging. The theory behind such "Cg" experiments is that differences between signal attenuation at a particular b value are directly related to restricted diffusion occurring in proton pools, with restrictions on the order of the diffusion time of the Cg experiment. The stretched exponential model may be used to understand the difference in monoexponentiality between constant-time (Ct) and Cg experiments, using the heterogeneity index α to determine the amount of local diffusive restrictions. Restrictions can be expected to result in an increase in the third moment of the distribution of β because the signal attenuation curve would be a result of protons that apparently diffuse more slowly than they would if diffusion time were held constant at a shorter value. Other effects could be explored as well, such as the sensitivity of α to such restrictions.

Based on the work presented here, the bi-exponential interpretation of signal attenuation in DWI gives concern. This conclusion is based on the observed lower SSR in 20% of voxels. We suggest that the use of the stretched-exponential model would be a suitable control for an experiment based on a biexponential model, since the former model (with fewer free parameters) is preferred if the two models are equally well fit. In addition, it has not yet been shown that the biexponential model directly corresponds to known physiology in the brain. It is possible, however, that a realistic model distinguishing between intra- and extracellular diffusion could be based on a sum of two stretched exponentials.

A stretched-exponential model of diffusion has been presented that enables the intravoxel heterogeneity in the distribution of diffusion coefficients, as measured with DWI, to be quantified. While some voxels may be composed of one or two separable distributions of proton pools, the assumption that diffusion takes place in one or two specific compartments is unwarranted when the number of contributing water pools is not known. Nevertheless, with the stretched-exponential model, some information about the distribution of diffusion coefficients can be obtained. This quantification of intravoxel heterogeneity will be particularly useful in studies of human tumor tissue, in which tortuous vasculature and heterogeneous cellular morphology may differentiate it from surrounding normal tissue.

ACKNOWLEDGMENTS

The authors received extensive support from K.J. Rebro and M.M. Kostenko in technical matters, and from B.K.Ventura and K.A. Hyde with figures and editing. The help of B.D. Ward was invaluable in simulations. S.W. Morgan and R.V. Mulkern provided helpful comments, as did A. Joseph, P.R. Kufahl, C.C. Quarles, Y. Mazaheri, and S.D. Rand.

REFERENCES

1. Kastrup A, Neumann-Haefelin T, Moseley ME, de Crespigny A. High speed diffusion magnetic resonance imaging of ischemia and spontaneous periinfarct spreading depression after thromboembolic stroke in the rat. J Cereb Blood Flow Metab 2000;20:1636–1647.
2. Maier CF, Paran Y, Bendel P, Rutt BK, Degani H. Quantitative diffusion imaging in implanted human breast tumors. Magn Reson Med 1997;37:576–581.
3. Lyng H, Haraldseth O, Rofstad EK. Measurement of cell density and necrotic fraction in human melanoma xenografts by diffusion weighted magnetic resonance imaging. Magn Reson Med 2000;43:828–836.
4. Darquie A, Poline J-B, Poupon C, Saint-Jalmes H, Le Bihan D. Transient decrease in water diffusion observed in human occipital cortex during visual stimulation. Proc Natl Acad Sci USA 2001;98:9391–9395.
5. Mulkern RV, Zengingonul HP, Robertson RL, Bogner P, Zou KH, Gudbjartsson H, Guttmann CR, Holtzman D, Kyriakos W, Jolesz FA, Maier SE. Multi-component apparent diffusion coefficients in human brain: relationship to spin-lattice relaxation. Magn Reson Med 2000;44:292–300.
6. Mulkern RV, Gudbjartsson WH, Westin CF, Zengingonul HP, Gartner W, Guttmann CR, Robertson RL, Kyriakos W, Schwartz R, Holtzman D, Jolesz FA, Maier SE. Multi-component apparent diffusion coefficients in human brain. NMR Biomed 1999;12:51–62.
7. Clark CA, Le Bihan D. Water diffusion compartmentation and anisotropy at high b values in the human brain. Magn Reson Med 2000;44:852–859.
8. Sehy JV, Ackerman JJH, Neil JJ. Apparent diffusion of water, ions, and small molecules in the *Xenopus* oocyte is consistent with Brownian displacement. Magn Reson Med 2002;48:42–51.

9. Sehy JV, Ackerman JJH, Neil JJ. Evidence that both fast and slow water ADC components arise from intracellular space. Magn Reson Med 2002;48:765–770.
10. Thewell PE, Grant SC, Stanisz GJ, Blackband SJ. Human erythrocyte ghosts: exploring the origins of multiexponential water diffusion in a model biological tissue with magnetic resonance. Magn Reson Med 2002;48:649–657.
11. Latour LL, Svoboda K, Mitra PP, Sotak CH. Time-dependent diffusion of water in a biological model system. Proc Natl Acad Sci USA 1994; 1229–1223.
12. Niendorf T, Norris D, Leibfritz D. Detection of apparent restricted diffusion in healthy rat brain at short diffusion times. Magn Reson Med 1994;32:672–677.
13. Quirk J, Bretthorst G, Neil J, Ackerman J. Measurement of transmembrane water exchange rate for in situ rat brain. In: Proceedings of the 9th Annual Meeting of ISMRM, Glasgow, Scotland, 2001. p 352.
14. Woolsey TA, van der Loos H. The structural organization of layer IV in the somatosensory region (S I) of mouse cerebral cortex. The description of a cortical field composed of discrete cytoarchitectonic units. Brain Res 1970;17:205–242.
15. Duvernoy HM. The human brain: surface, three-dimensional sectional anatomy with MRI, and blood supply, 2nd ed. New York: Springer-Verlag; 1999. p 455.
16. Pfeuffer J, Provencher SW, Gruetter R. Water diffusion in rat brain in vivo as detected at very large b values is multicompartmental. MAGMA 1999;8:98–108.
17. Rabaini E, Gezelter JD, Berne BJ. Direct observation of stretched-exponential relaxation in low-temperature Lennard-Jones systems using the cage correlation function. Phys Rev Lett 1999;82:3649–3652.
18. Hartman SJ, Narayanan A, Wang Y. Spin-lattice relaxation in the 6H polytype of silicon carbide. J Am Chem Soc 1994;116:4019–4027.
19. Narayanan A, Hartman JS, Bain AD. Characterizing nonexponential spin-lattice relaxation in solid-state NMR by fitting to the stretched exponential. J Magn Reson Ser A 1995;112:58–65.
20. Henrichs PM, Cofield ML, Young RH, Hewitt JM. Nuclear spin-lattice relaxation via paramagnetic centers in solids. 13C NMR of diamonds. J Magn Reson 1984;58:85–94.
21. Benny Lee KC, Siegel J, Web SED, Leveque-Fort S, Cole MJ, Jones R, Dowling K, Lever MJ, French PMW. Application of the stretching exponential function to fluoresence lifetime imaging. Biophys J 2001; 81:1265–1274.
22. Alvarez F, Alegria A, Colmenero J. Relationship between the time-domain Kohlrausch-Williams-Watts and frequency-domain Havriliak-Negami relaxation functions. Phys Rev Series B 1991;44:7306–7312.
23. Kopf M, Corinth C, Haferkamp O, Nonnenmacher TF. Anomolous diffusion of water in biological tissues. Biophys J 1996;70:2950–2958.
24. Paxinos G. The rat nervous system, 2nd ed. San Diego, CA: Elsevier; 1994.
25. Bennett K, Cox RW, Lu H, Schmainda K, Bennett R, Hyde JS. A measure of restricted water diffusion in neural. In: Proceedings of the 9th Annual Meeting of ISMRM, Glasgow, Scotland, 2001. p 1515.
26. Pfeuffer J, Flogel U, Dreher W, Leibfritz D. Restricted diffusion and exchange of intracellular water: theoretical modeling and diffusion time dependence of 1H NMR measurements on perfused glial cells. NMR Biomed 1998;11:19–31.
27. Pfeuffer J, Flogel U, Leibfritz D. Monitoring of cell volume and water exchange time in perfused cells by diffusion-weighted 1H NMR spectroscopy. NMR Biomed 1998;11:11–18.
28. Callaghan PT. Principles of nuclear magnetic resonance microscopy. Oxford, UK: Oxford University Press; 1993.
29. Assaf Y, Cohen Y. Structural information of neuronal tissue as revealed by q-space diffusion NMR spectroscopy of metabolites in bovine optic nerve. NMR Biomed 1998;11:67–64.
30. Assaf Y, Cohen Y. Assignment of the water slow-diffusion component in the central nervous system using q-space diffusion MRS: implications for fiber tract tracing. Magn Reson Med 2000;43:191–199.
31. Lythgoe MF, Busza AL, Calamante F, Sotak CH, King MD, Bingham AC, Williams SR, Gadian DG. Effects of diffusion anisotropy on lesion delineation in a rat model of cerebral ischemia. Magn Reson Med 1997;38:662–668.
32. Hoehn-Berlage M, Eis M, Schmitz B. Regional and directional anisotropy of apparent diffusion coefficient in rat brain. NMR Biomed 1999; 12:45–50.